

Nonlinear critical-layer evolution of a forced gravity wave packet

By L. J. CAMPBELL¹† AND S. A. MASLOWE²

¹Department of Physics, University of Toronto, Toronto, Ontario, Canada, M5S 1A7

²Department of Mathematics and Statistics, McGill University, Montréal, Québec, Canada, H3A 2K6

(Received 9 July 2002 and in revised form 20 May 2003)

In this paper, numerical simulations are presented of the nonlinear critical-layer evolution of a forced gravity wave packet in a stratified shear flow. The wave packet, localized in the horizontal direction, is forced at the lower boundary of a two-dimensional domain and propagates vertically towards the critical layer. The wave–mean-flow interactions in the critical layer are investigated numerically and contrasted with the results obtained using a spatially periodic monochromatic forcing. With the horizontally localized forcing, the net absorption of the disturbance at the critical layer continues for large time and the onset of the nonlinear breakdown is delayed compared with the case of monochromatic forcing. There is an outward flux of momentum in the horizontal direction so that the horizontal extent of the packet increases with time. The extent to which this happens depends on a number of factors including the amplitude and horizontal length of the forcing. It is also seen that the prolonged absorption of the disturbance stabilizes the solution to the extent that it is always convectively stable; the local Richardson number remains positive well into the nonlinear regime. In this respect, our results for the localized forcing differ from those in the case of monochromatic forcing where significant regions with negative Richardson number appear.

1. Introduction

It has been recognized for many years that instability and wave motion in stratified shear flows play an important role in atmospheric phenomena such as clear air turbulence, stratospheric sudden warmings and the quasi-biennial oscillation. It is also believed that in thermocline regions of the ocean the momentum and energy exchanged between internal gravity waves and currents is considerable. The principal parameter in the linear stability theory of stratified flows is the Richardson number Ri , which is essentially the ratio of the stabilizing buoyancy effect to the destabilizing effect of shear. In our numerical simulations, the initial mean flow Ri is everywhere greater than $1/4$, so the mean flow is stable according to the Miles–Howard theorem. For small-amplitude gravity waves on a parallel shear flow $\bar{u}(z)$, the second-order Taylor–Goldstein amplitude equation results when the normal mode approach is employed. This equation is singular at the height where $\bar{u}(z) = c$, the perturbation phase speed. By expanding in power series around the critical point z_c , Miles (1961)

† Present address: School of Mathematics and Statistics, Carleton University 1125 Colonel By Drive, Ottawa, Ontario, Canada, K1S 5B6; campbell@math.carleton.ca

was able to determine expressions for the Reynolds stress on either side of the critical point. These are, in general, different owing to discontinuities in the eigenfunctions (i.e. the phase change of hydrodynamic stability theory).

Within the framework of linear theory, the phase change can be determined in two different ways, each of which leads to the same result. The first way involves introducing viscosity and heat conduction in a critical layer of thickness $O(\alpha Re)^{-1/3}$, where α is the disturbance wavenumber and Re the Reynolds number. The second method is to use transforms instead of normal modes to solve the initial-value problem for the linearized vorticity equation. In general, a Fourier transform in x and a Laplace transform in time are required, but only the Laplace transform is required to obtain the phase change. This method was used by Booker & Bretherton (1967) in their study of forced gravity waves propagating vertically towards a critical level. In both cases, a phase change of $-\pi$ is found. In the case of forced waves, the phase change and the discontinuity in the solution imply that the waves are effectively absorbed by the mean flow in the critical layer. The vertical flux of horizontal momentum, which would have been independent of height in the absence of a critical level (Eliassen & Palm 1961), is reduced across the critical layer by a factor of $\exp\{-2\pi(Ri_c - 1/4)\}$, where Ri_c is the Richardson number at the critical level. As the time $t \rightarrow \infty$, however, the analysis breaks down in the critical layer. This is because both the horizontal perturbation velocity and the density perturbation become infinite at the critical level so that nonlinearity must be taken into account.

There has been some analytical work that extends the analysis of Booker & Bretherton into the nonlinear regime. In the last of a series of three papers, Brown & Stewartson (1982) found evidence of a weak transmitted wave in addition to a considerably stronger reflected wave. They obtained improved asymptotic representations of the linear solution and then used these to attack the nonlinear, time-dependent critical-layer equations by means of an expansion in powers of a slow time variable $\tau = \alpha \varepsilon^{2/3} t$, where α is the horizontal wavenumber and ε is the non-dimensional amplitude of the perturbation. Insights were provided by this work concerning the detailed interactions within the critical layer, but the analysis is limited to times $\tau \ll Ri_c^{1/6}$.

The aforementioned studies were all based on the assumption that the disturbance is periodic in the horizontal direction. However, a more realistic representation of the behaviour of gravity waves in the atmosphere or ocean can be obtained by employing a forcing in the form of a horizontally localized wave packet with an amplitude that varies slowly in space. A monochromatic periodic forcing can be justified only if the wavelength of the disturbance is assumed to be of the order of magnitude of the circumference of the earth. However, for a disturbance that is not on this scale, there is no reason to assume periodicity. This is especially true for simulations of orographically forced gravity waves since, in reality, a mountain range would be of finite length only and would not be monochromatic.

The behaviour of a stratified fluid flowing over a horizontally localized obstacle such as an isolated mountain has received a considerable amount of attention in recent decades. The main motivation for many of these studies was to understand the mechanism that leads to downslope windstorms. Observations show that the drag force on an isolated obstacle is, in general, higher than that predicted by linear theory and theoretical studies of the nonlinear dynamics of the flow in the vicinity of the obstacle (e.g. Peltier & Clark 1979) show that this high-drag state is due to the deposition of momentum in the mean flow by lee waves breaking downstream. The mechanism for the wave breaking was attributed to critical-layer interactions and, for this reason, several workers (e.g. Clark & Peltier 1984; Bacmeister & Pierrehumbert

1988) have investigated the effect of the presence of a critical layer in the flow. Clark & Peltier examined the case in which the critical level is at a specific height above the ground that allows resonance between the waves incident on it and the reflected waves. They showed that the drag force exerted on the obstacle would depend on the height of the critical level. This result was arrived at by assuming the flow to be linear everywhere outside the critical layer and also that the critical layer would act as a perfect reflector. However, Bacmeister & Pierrehumbert (1988) pointed out that there was no justification for ruling out the possibility of critical-layer absorption; they showed that, not only could there be absorption, but that the absorbing state could even continue indefinitely. They calculated the vertical momentum flux and noted that it was discontinuous across the critical layer, as shown by Booker & Bretherton (1967) and other earlier workers. This discontinuity was balanced by a change in the horizontal momentum flux across the region above the obstacle so that there was zero net flux in the region above the forcing. Absorption of the incident waves was prolonged, with the disturbance propagating horizontally within the critical layer.

It must be noted that the possibility of prolonged critical-layer absorption of a wave packet was later suggested by Brunet & Haynes (1996) in the context of a Rossby wave packet propagating horizontally towards a nonlinear critical layer, although their numerical simulations showed net reflection of the packet at late time. Late-time absorption of a forced Rossby wave packet was seen in the nonlinear critical-layer study of Campbell (2003). Numerical simulations and an asymptotic analysis showed that the extent of absorption, relative to reflection, depends on a number of factors, including the length and amplitude of the packet at the source.

For the case of gravity wave packets, it would be of interest to see if the absorbing state observed by Bacmeister & Pierrehumbert obtains in general or if it only occurs in the particular configuration that was used in their study, i.e. a Gaussian forcing. Although there are numerous analogies between the two problems (horizontally propagating Rossby waves in a zonal shear flow and vertically propagating gravity waves in a stratified flow), there is no reason to assume *a priori* that the conclusions of Campbell (2003) can necessarily be extended to gravity wave packets. A separate investigation of the nonlinear gravity wave packet critical layer is needed to determine the factors that determine the late-time absorption/reflection behaviour of the critical layer.

Another possibility is that there could be non-negligible transmission of wave activity through the critical layer, as in the case examined by Javam & Redekopp (1998). The gravity wave packet in their study was of finite length in the horizontal direction and its amplitude took the form of a step-function; their forcing function, however, differed from that employed here in the sense that it was localized in the vertical direction as well as in the horizontal. Their numerical simulations showed that if the wave packet was sufficiently compact, a significant portion of its energy would be transmitted through the critical level.

In this paper, we examine the nonlinear critical layer for a horizontally localized gravity wave packet, focusing on two main issues. The first is to determine which of the different possibilities dominates in the critical layer at late time: absorption, reflection or even perhaps transmission. In our simulations, we employ a periodic forcing of wavenumber k whose amplitude is modulated in the horizontal x -direction by a Gaussian factor $\exp(-\mu^2 x^2)$, where μ is a small parameter. Setting $k = 0$ would correspond to an isolated mountain. The results of the simulations show that, even at late time, absorption dominates over reflection and transmission. The horizontal extent of the packet increases with time in the critical layer, which is in agreement

with the observations of Bacmeister & Pierrehumbert for waves forced by flow over an isolated obstacle. The extent to which this happens depends on the relative magnitude of the two important parameters, μ which determines the length of the packet at the source level and ε , the nonlinear parameter which measures the amplitude of the forcing.

It will be seen here that, in the critical layer, the zero-wavenumber component of the disturbance is several orders of magnitude larger than the contributions from higher wavenumbers. To understand why this is so, we re-examine the analytic solution of Booker & Bretherton (1967) and investigate the effect of adding the nonlinear terms and the spatial localization of the forcing to their solution. From this, we can compare the order of magnitude of the different components of the solution.

The second issue addressed here concerns the possibility of secondary instabilities developing in the critical layer at late time. For linear disturbances, it is well-known that instabilities can occur only if $Ri < 1/4$ somewhere in the flow (Howard 1961; Miles 1961) and this criterion is often extended and applied to time-dependent problems as well. Negative values of Ri indicate unstable stratification and the possibility of convective instabilities. The question of whether secondary instabilities in nonlinear critical layers are the result of regions in which $Ri < 0$ or $Ri < 1/4$ has been the subject of considerable debate during the past 20 years. Fritts (1982), Winters & D'Asaro (1989) and Lin *et al.* (1993) addressed this issue in the context of disturbances that are monochromatic in the horizontal direction but localized in the vertical direction. Fritts found regions where $Ri < 0$, while Winters & D'Asaro found regions where $0 < Ri < 1/4$. Lin *et al.* used high-resolution simulations to show that at late time both convective and dynamical instabilities develop. In our simulations, we shall see that, with a monochromatic forcing, regions in which $Ri < 0$ and $0 < Ri < 1/4$ develop eventually. However, when a horizontally localized forcing is employed, the local Richardson number remains positive even at late time.

In the next section, the equations used in our study are described. The configuration and choice of parameters used and the results of the numerical simulations are discussed in §3. In the simulations, a radiation condition is implemented at the upper boundary of the computational domain; this is described in Appendix A. Further insight into some of the features of the numerical solutions is obtained by examining the approximate analytical solution to the governing equations. An outline of the procedure used to derive the approximate solution is given in Appendix B. Some concluding remarks are given in §4.

2. The governing equations

We examine the evolution of an internal gravity wave packet propagating vertically upwards in a stratified shear flow in a two-dimensional region defined by the coordinates x and z in the horizontal and vertical directions, respectively. All the variables and parameters are non-dimensionalized with respect to typical length scales L_x and L_z in the x - and z -directions, a typical density scale, a typical velocity scale, U , and the dimensional amplitude, φ , of the perturbation streamfunction at the source.

We make the Boussinesq approximation, i.e. take into account density variations only in the terms in the governing equations involving buoyancy forces. The background density and velocity are denoted by $\bar{\rho}(z)$ and $\bar{u}(z)$ and the perturbation streamfunction, vorticity and density by $\psi(x, z, t)$, $\zeta(x, z, t)$ and $\rho(x, z, t)$, respectively. The streamfunction is defined in terms of the disturbance velocity (u, w) by $u = -\psi_z$ and

$w = \psi_x$. The governing equations for the evolution of the perturbation are

$$\zeta_t + \bar{u}\zeta_x - \bar{u}''\psi_x + g(\bar{\rho})^{-1}\rho_x + \varepsilon(\psi_x\zeta_z - \psi_z\zeta_x) - Re^{-1}\nabla^2\zeta + Re^{-1}\varepsilon^{-1}\bar{u}''' = 0, \quad (2.1)$$

where

$$\zeta = \nabla^2\psi \quad (2.2)$$

and

$$\rho_t + \bar{u}\rho_x + \bar{\rho}'\psi_x + \varepsilon(\psi_x\rho_z - \psi_z\rho_x) - Re^{-1}Pr^{-1}\nabla^2\rho - Re^{-1}Pr^{-1}\varepsilon^{-1}\bar{\rho}'' = 0. \quad (2.3)$$

Here, the primes denote differentiation with respect to z while the subscripts x and z denote partial differentiation. The Laplacian operator is non-dimensional with the x -derivative in the operator multiplied by a factor $\delta = L_z^2/L_x^2$, which is the square of the aspect ratio. The parameter ε is defined as $\varphi/(L_z U)$ and gives a measure of the amplitude of the disturbance at the source. It is assumed that $\varepsilon \ll 1$. The constant g is the acceleration due to gravity and Re and Pr are the Reynolds number and Prandtl number, respectively; it is assumed that $Re \gg 1$ and Pr is set to 0.72, the value of the Prandtl number for air. The last term in each of equations (2.1) and (2.3) must be included because the mean density and velocity profiles used in our simulations do not satisfy the equations with the viscous and heat conduction terms included.

In our numerical simulations, the disturbance is generated by a forcing applied at the lower boundary z_1 of the computational domain. Two types of forcing function are used: a periodic forcing of the form $e^{ikx} + \text{c.c.}$ and a horizontally localized forcing of the form

$$\psi(x, \mu x, z_1, t) = A(\mu x, t)e^{ikx} + \text{c.c.} \quad (2.4)$$

In (2.4), μ is assumed to be a small parameter, so that the amplitude A of the forcing varies slowly with x .

The question arises as to how we should define the ‘mean’ flow when the forcing takes the form (2.4). In the case of the periodic forcing, the mean is taken to be an average over a horizontal wavelength $2\pi/k$. However, this definition cannot be used in the horizontally localized case, where the disturbance varies slowly with x and has a different amplitude over each wavelength interval. In the horizontally localized case, the most appropriate definition of the ‘mean’ would be an average taken over a length L equal to the non-dimensional length of the packet. The packet length, however, increases with time, as we shall see in §3, so L must be chosen to be of the same order of magnitude as the non-dimensional length of the packet at the forced boundary, but large enough that the packet is completely contained within an interval of length L at all times. In the numerical simulations, L is chosen to be approximately the length of the computational domain.

The horizontally localized perturbation may be expressed as a Fourier integral

$$\psi = \int_{-\infty}^{\infty} \hat{\psi}(\kappa, z, t) e^{ikx} d\kappa, \quad (2.5)$$

and the wave-induced mean flow then corresponds to the zero wavenumber term in the integrand, i.e. the wave-induced mean streamfunction is

$$\bar{\psi}_0(z, t) = \frac{\varepsilon}{L} \int_{-\infty}^{\infty} \psi dx = \frac{\varepsilon}{L} \hat{\psi}(0, z, t) \quad (2.6)$$

and the wave-induced horizontal velocity is $\bar{u}_0(z, t) = -\bar{\psi}_{0z}$. In a similar manner, other quantities that would, in the periodic problem, be defined as averages over a

wavelength, are evaluated instead by integrating over the length of the packet. For example, the averaged vertical momentum flux is defined as

$$F = -\frac{1}{L} \int_{-\infty}^{\infty} \bar{\rho} u w \, dx. \quad (2.7)$$

In the wave-packet problem, taking an average over the length of the packet gives us information about the zero wavenumber component of the disturbance only. However, there is a continuous spectrum of wavenumbers and it is of interest to know how the components of the disturbance corresponding to the different wavenumbers evolve with time. For this reason, we shall also make use of the following decomposition in which the part of the disturbance that depends directly on the fast scale x , i.e. the periodic part of the disturbance, is separated from the slowly varying part. The perturbation streamfunction is written as

$$\psi(x, z, t) = \psi_0(\mu x, z, t) + \varepsilon \psi_1(x, \mu x, z, t). \quad (2.8)$$

The function ψ_0 is a long wave comprised of contributions from wavenumbers κ in a small neighbourhood of the zero wavenumber. It varies slowly with x , so we may think of it as a function of μx , which does not depend explicitly on the fast x scale. The function ψ_1 is comprised of contributions from the higher wavenumbers. In practice, such a decomposition is accomplished by dividing the range of integration ($-\infty < \kappa < \infty$) of the Fourier integral (2.5) into subintervals and evaluating the integral over each subinterval separately. Evaluating the integral over the low wavenumbers gives ψ_0 , while evaluating it over higher wavenumbers gives ψ_1 . This is described in more detail in § 3.2.

3. Numerical simulations

3.1. Configuration

The numerical simulations were carried out on a rectangular domain defined by $x_1 \leq x \leq x_2$ and $z_1 \leq z \leq z_2$. The forcing was applied at the lower boundary, $z_1 = 0$, and was of the form

$$\psi = e^{-\mu^2 x^2} e^{ikx} f(t) + \text{c.c.}, \quad (3.1)$$

where

$$f(t) = \begin{cases} t/t_1, & t < t_1, \\ 1, & t \geq t_1, \end{cases} \quad (3.2)$$

with t_1 constant and μ a small parameter. For comparison with earlier studies such as Booker & Bretherton (1967), computations with monochromatic forcing ($\mu = 0$) were also carried out. With this forcing function, the amplitude of the disturbance at z_1 was increased with time from zero at $t = 0$ and then kept fixed after a certain time $t = t_1$. The reason for this slow ‘switch-on’ of the forcing was to prevent instabilities from developing near the inflow boundary, which could occur if the time step used in the numerical solution was not sufficiently small.

The initial velocity and density profiles were taken to be $\bar{u} = \tanh \alpha_0(z - z_c)$ (shown in figure 1) and $\bar{\rho} = \rho_0 e^{-z/h}$, respectively, where α_0 , ρ_0 , h and z_c are non-dimensional constants and z_c , the location of the critical level, was set to 5. At the upper boundary ($z_2 = 10$), a radiation condition was applied to allow any waves transmitted beyond the critical layer to propagate out of the computational domain on reaching the boundary. This is described in Appendix A.

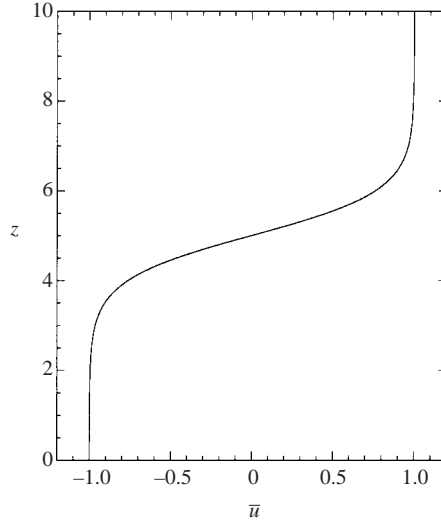


FIGURE 1. Initial mean velocity profile used in the standard run: $\bar{u} = \tanh \alpha_0(z - z_c)$ with $z_c = 5$ and $\alpha_0 = 1$. This gives $Ri_c = 2$. In the large Ri_c experiment shown in figure 15, α_0 is set to 0.5. In all our simulations, the forcing is applied at the lower boundary where $\bar{u} \approx -1$.

There were a number of restrictions on the choice of the various non-dimensional parameters used in the simulations. In particular, they had to be chosen in such a way that the disturbance would be able to propagate towards the critical layer without amplification or attenuation. In the region near the forced boundary, the disturbance is linear and steady and so normal mode expressions can be assumed for the perturbation streamfunction and density. Writing ψ as $\phi(z) e^{ik(x-ct)} + \text{c.c.}$, with k and c real, and a similar expression for ρ , we obtain the Taylor–Goldstein equation,

$$\phi_{zz} + \left(\frac{N^2}{(\bar{u} - c)^2} - \frac{\bar{u}''}{\bar{u} - c} - \delta k^2 \right) \phi = 0, \quad (3.3)$$

where N is the Brunt–Väisälä frequency, defined by

$$N^2 = \frac{-g}{\bar{\rho}} \frac{\partial \bar{\rho}}{\partial z}. \quad (3.4)$$

Near the forced boundary, the mean velocity is almost constant ($\bar{u} \approx -1$ and $\bar{u}'' \approx 0$), so the WKB method can be applied to this equation to determine the appropriate range of values of the parameters. For this equation to have periodic solutions near the forced boundary, we must have $N^2 - \delta k^2 > 0$. The important parameter to measure the relative importance of viscosity to nonlinearity in the critical layer is generally denoted as λ . This is defined to be the cube of the ratio of the thickness of the critical layer according to the viscous theory ($Re^{-1/3}$) to that in the nonlinear theory ($\varepsilon^{2/3}$) (Maslowe 1972). In all our simulations, we set $\lambda \ll 1$.

Based on these restrictions, a set of parameters was chosen for a standard run and the results were used for comparison with the results obtained by varying the different parameters. We set $\rho_0 = 1.0$, $\alpha_0 = 1.0$ and the density scale height $h = 4.9$, so that $N^2 = 2$. The initial Richardson number is $Ri = N^2/(\bar{u}')^2 = 2$; its minimum value occurs at the critical level z_c and is denoted by Ri_c . With this configuration, $Ri_c = 2$ and so the flow is stable everywhere, at least initially, according to the Miles–Howard

theorem. We also set $\varepsilon = 0.05$, $\lambda = 0.1$, the square of the aspect ratio $\delta = 0.2$ and the wave-packet parameter $\mu = 0.2$, with the forcing centred at wavenumber $k = 2$. With this choice of μ and k , the length of the packet at the forced boundary is approximately 20 non-dimensional units and the wavelength is approximately π units, so that there are several wave oscillations within the packet length. The horizontal extent of the computational domain was chosen to be large enough to ensure that the amplitude of the disturbance would decay to zero at the boundaries at all times; in general, an interval within the range $-30 \leq x \leq 30$ was sufficient. The calculations with monochromatic forcing were carried out with the same set of parameter values, but over the interval $0 \leq x \leq 2\pi$ and with periodic boundary conditions.

Equations (2.1)–(2.3) were solved numerically by taking a Fourier transform in the x -direction and then solving the transformed equations numerically, with the nonlinear terms calculated using a pseudospectral method. The Fourier integrals were evaluated using a trapezoidal approximation and a variation of the fractional Fourier transform method (Bailey & Swarztrauber 1991, 1994). This method is a generalization of the standard fast Fourier transform (FFT) algorithm that allows greater flexibility in the choice of the computational domain in both physical and wavenumber space. The application of the method to our problem is described in Campbell (2000).

The derivatives in the vertical direction were approximated using fourth-order compact finite differences. These methods have a number of advantages over other methods of comparable accuracy: they give a better representation of short length scales than traditional finite-difference schemes and for that reason are comparable to spectral methods (see, for example, Lele 1992). The finite-difference mesh was non-uniform with a very fine mesh in the critical-layer region, a coarser mesh in the region above and intermediate spacing below. Derivatives on the non-uniform mesh were evaluated by first calculating them on a uniform mesh and then transforming them into derivatives on the non-uniform mesh. A description of the procedure is given by Campbell & Maslowe (2001). The choice of $\varepsilon = 0.05$ gives a nonlinear critical-layer thickness of $\varepsilon^{2/3} \approx 0.136$ non-dimensional units. By experimenting with the mesh spacing, reducing it until the computed solution was found to be independent of the mesh size, it was found that a minimum of about 20 points was needed in the critical layer to represent the evolution of the disturbance accurately. The time derivatives were discretized using the second-order Adams–Bashforth method and the time-step size was set to 0.02 non-dimensional units, a value small enough to ensure stability of the computations.

3.2. *The results of the standard run*

Numerical simulations with the standard set of parameters ($\varepsilon = 0.05$, $\lambda = 0.1$, $\mu = 0.2$, $Ri_c = 2$) were carried out over the time interval $t = 0$ to $t = 100$. The results are shown in figures 2–11. Figures 2 and 3 show contour plots of the horizontal velocity perturbation $u(x, z, t) = -\psi_z$ at early time ($t = 10$) and late time ($t = 100$) with the two different types of forcing. In figures 2(a) and 3(a), it is seen that there is almost complete absorption of the disturbance at the critical level at early time. The late-time plots 2(b) and 3(b) show modifications of the contours below the critical layer; this is because some reflection of the incident disturbance is taking place and the downward-propagating reflected waves are superimposed on top of the incident waves. In figure 2(b), the horizontal extent of the packet has increased considerably, both in the outer region and in the critical layer; in these extended regions, the dominant modes are clearly the low wavenumbers.

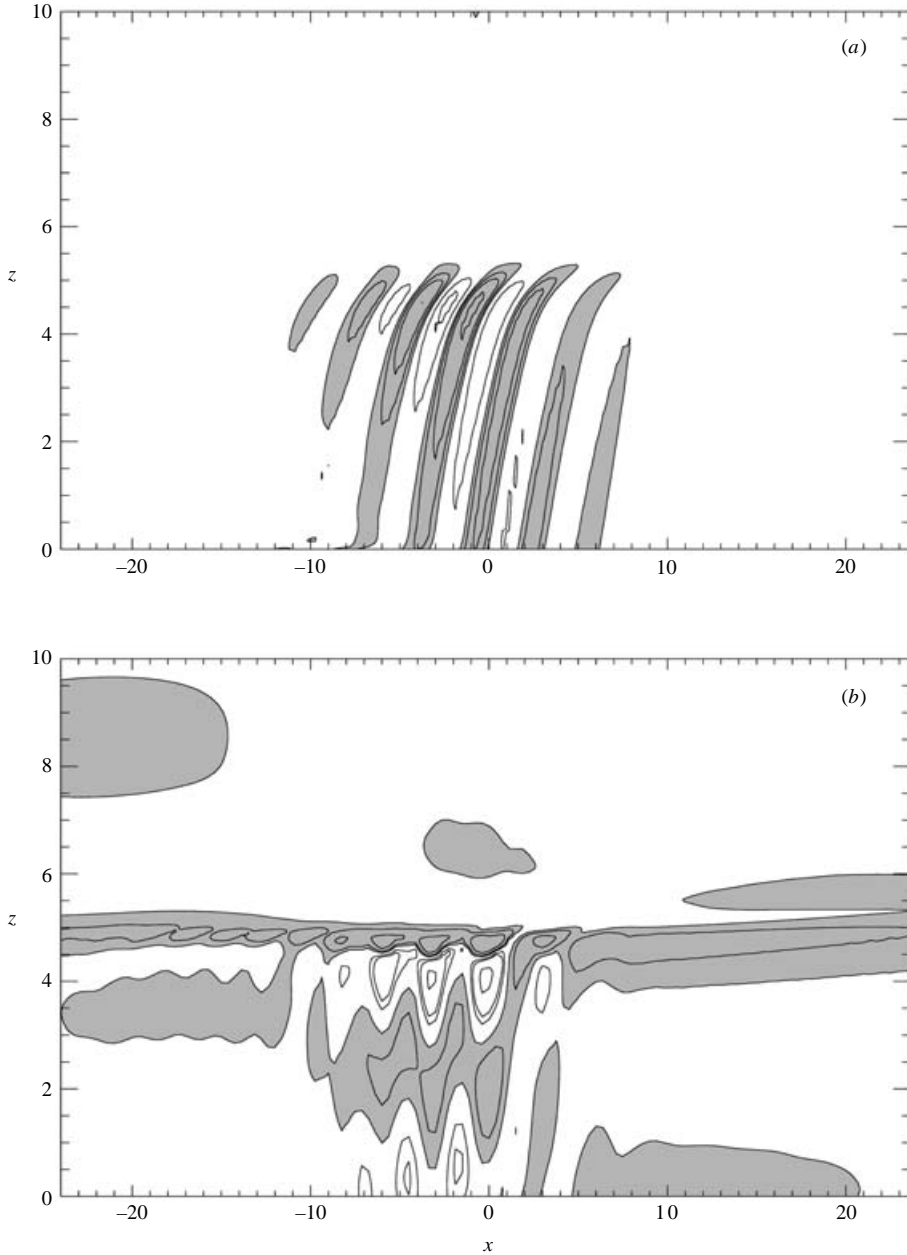


FIGURE 2. Wave packet forcing: horizontal velocity perturbation as a function of x and z at (a) $t=10$ and (b) $t=100$. Parameters: $\varepsilon=0.05$, $\lambda=0.1$, $\mu=0.2$, $Ri_c=2$. Contour levels range from -2 to a maximum of 10 in the critical layer at $t=100$. Regions where $u > 0$ are shaded. At early time (a), there is almost complete net absorption of the disturbance at the critical level ($z=5$). At late time (b), the contour pattern is modified below the critical level as a result of reflections.

The simplest way to measure the extent of reflection or absorption of the disturbance is to examine the behaviour of the vertical momentum flux (2.7) in the vicinity of the critical layer. This was seen to be discontinuous across the critical layer, almost constant (negative) below and zero above. At each time step, the jump $[F]$ across

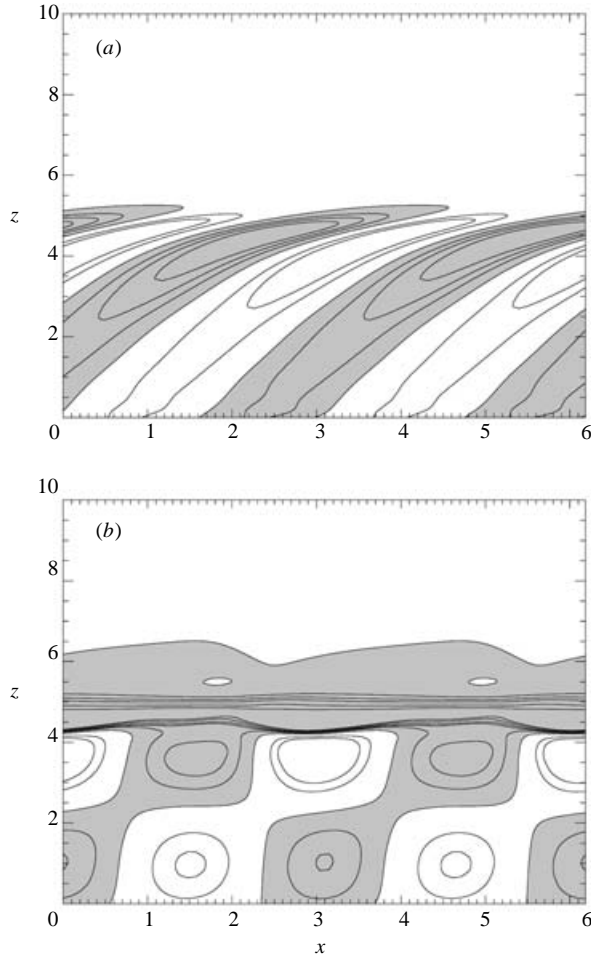


FIGURE 3. Monochromatic forcing: horizontal velocity perturbation as a function of x and z at (a) $t = 10$ and (b) $t = 100$. Parameters: $\varepsilon = 0.05$, $\lambda = 0.1$, $Ri_c = 2$. Contour levels range from -2 to a maximum of 10 in the critical layer at $t = 100$. Regions where $u > 0$ are shaded. At early time (a), there is almost complete net absorption of the disturbance at the critical level ($z = 5$). At late time (b), the contour pattern is modified below the critical level as a result of reflections.

the critical layer was calculated, normalized by the maximum value $[F]_{max}$ that it attained and the result plotted as a function of time. This is shown in figure 4 for both types of forcing. When ε is set to zero for the duration of the calculation, the jump increases initially during the switch-on time, but eventually attains a steady state. This is shown by the thin solid line and the dotted line for the wave-packet forcing and the monochromatic forcing, respectively. In the nonlinear simulations (shown by the thick solid line for the wave-packet forcing and by the dashed line for the monochromatic forcing), the early-time evolution of $[F]$ is as in the linear case; however, no steady state is attained and the nonlinear effects soon become evident as $[F]$ starts to decrease rapidly. According to the nonlinear (inviscid) critical-layer theory of Brown & Stewartson (1982), we would expect the nonlinear regime to start around the time that $t \sim O(\varepsilon^{-2/3})$. With our choice of $\varepsilon = 0.05$, this would be as early as $t = 7$; however, with the inclusion of viscosity, it could be expected that it would be delayed slightly.

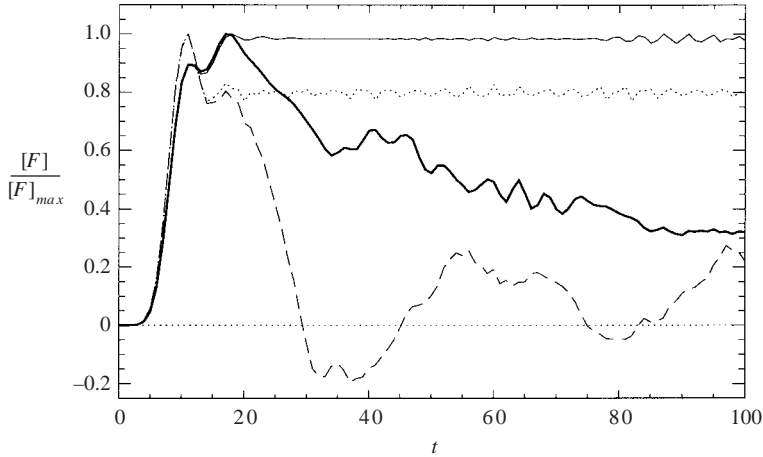


FIGURE 4. Variation of the jump in the (normalized) momentum flux with t . Comparison of results obtained with wave packet forcing ($\mu = 0.2$) and monochromatic forcing ($\mu = 0$). The thick solid line shows the results obtained with the wave packet forcing ($\mu = 0.2$), the dashed line with monochromatic forcing ($\mu = 0$). Parameters: $\varepsilon = 0.05$, $\lambda = 0.1$, $Ri_c = 2$. For the wave packet forcing, the corresponding curve obtained with $\varepsilon = 0$ is shown by the thin solid line; for the monochromatic forcing, it is shown by the dotted line. The level $[F]/[F]_{max} = 0$ has also been indicated with a dotted line.

With both types of forcing, the nonlinear effects are first seen at around $t = 14$ when the linear curves no longer coincide exactly with the corresponding nonlinear curves. From that point on, the difference in the evolution of the momentum flux between the periodic and the wave-packet results becomes apparent. In the periodic problem, the jump drops rapidly to zero and to negative values, indicating first reflection and then over-reflection of the waves, and then continues to oscillate between these states. In contrast, with the wave packet forcing, although the jump in the momentum flux decreases, it remains positive all the way up to the end of the simulation. This means that, although there is some reflection, the extent of absorption is much larger and there is net absorption of momentum flux into the critical layer.

For the wave-packet forcing, the vertical momentum flux has been plotted in figure 5(a) as a function of z at time $t = 100$. This corresponds to the end of the simulation indicated by the thick solid line in figure 4. Also shown is the wave-induced mean velocity \bar{u}_0 at that same time (figure 5b). The corresponding quantities evaluated at early time ($t = 10$) are shown by the dashed lines. The positive jump in the momentum flux across the critical layer means that a positive drag force is exerted on the mean flow and the mean velocity is accelerated, i.e. the mean velocity distortion \bar{u}_0 , defined below (2.6), is positive. With the wave packet forcing, the mean velocity continues to be accelerated in the critical layer at late time, in contrast to the monochromatic case where it alternates between periods of acceleration and deceleration. Away from the critical layer where the momentum flux is almost independent of height, \bar{u}_0 is close to zero.

The net absorption of the disturbance continues at late time because the horizontal extent of the disturbance increases with time. The increased extent of the disturbance is due mainly to the contribution from the neighbourhood of the zero wavenumber; this is seen in figure 2(b) by the absence of horizontal oscillations everywhere except in the central region, $-5 < x < 5$, between the forcing and the critical level. The extent

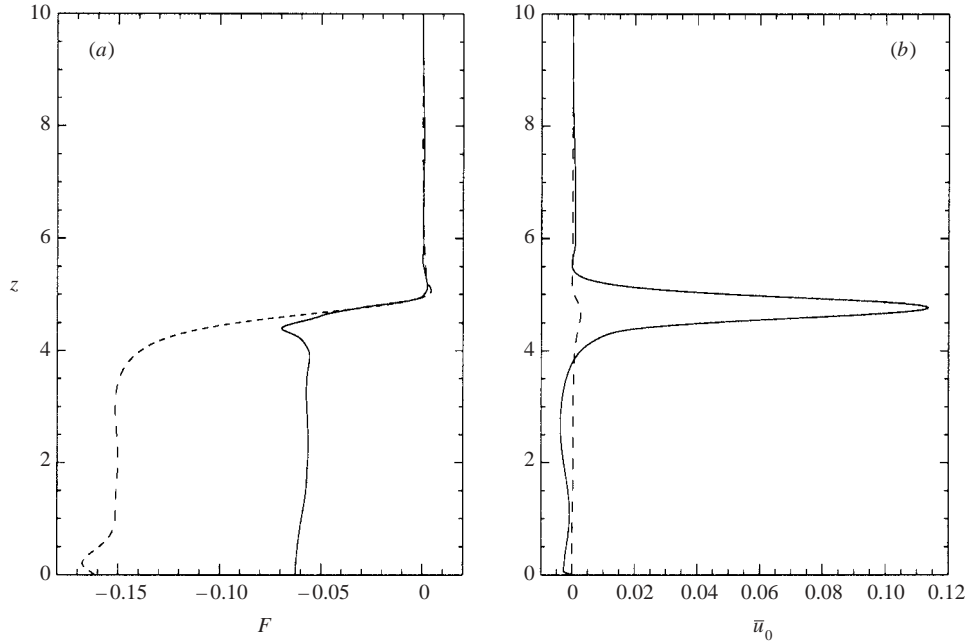


FIGURE 5. Wave packet forcing: variation with z of (a) the mean vertical momentum flux $F(z, t)$ and (b) the wave-induced mean velocity $\bar{u}_0(z, t)$. Parameters: $\varepsilon = 0.05$, $\lambda = 0.1$, $\mu = 0.2$, $Ri_c = 2$. The dashed lines show results obtained at $t = 10$, the same time as in figure 2(a); the solid lines show results obtained at $t = 100$, the same time as in figure 2(b).

to which the zero wavenumber contribution dominates the contributions from the forced wavenumber and the higher harmonics in the critical layer is seen more clearly in figure 6. The Fourier spectra of the streamfunction and the density at z_c are shown as functions of wavenumber κ . The Fourier transform of each quantity is denoted by a hat. The increased horizontal extent of the packet is seen in figure 6(b) by the narrowing of the peaks at $\kappa = 0$ and $\kappa = \pm 2$ compared with their width during the linear regime.

To investigate this further, we examined the part of the disturbance arising from the wavenumbers in the immediate vicinity of the zero wavenumber. This is the term $\psi_0(\mu x, z, t)$, defined in equation (2.8). The corresponding quantity for the velocity shall be denoted as $u_0(\mu x, z, t)$. To evaluate these, we calculated the inverse Fourier transforms of $\hat{\psi}(\kappa, z, t)$ and $-\hat{\psi}_z(\kappa, z, t)$, restricting the computations to wavenumbers in the neighbourhood of $\kappa = 0$, i.e. wavenumbers in the interval $|\kappa| < 1$. The quantity $u_0(\mu x, z, t)$ evaluated at the critical level at time $t = 100$ is shown in figure 7 as a function of x . The wave-induced mean velocity $\bar{u}_0(z, t)$ at that level would be the x -average of $u_0(\mu x, z, t)$ over the length of the computational domain. For fixed x , u_0 plotted as a function of z takes a similar form to the mean quantity \bar{u}_0 which is shown in figure 5(b), i.e. it is close to zero away from the critical layer, positive in the critical layer, attains its maximum near the critical level and this maximum grows larger with time.

In a similar manner, we can calculate the component of the disturbance corresponding to the higher wavenumbers, as defined in (2.8). We shall go further than (2.8) and decompose the disturbance into three parts, by evaluating the Fourier integral (2.5) over three subintervals: the range of low wavenumbers, the range of wavenumbers

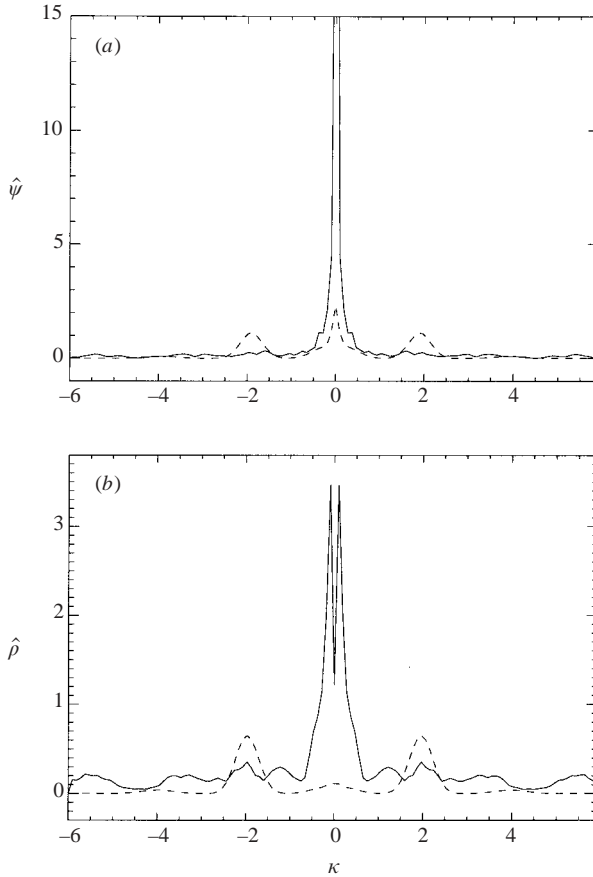


FIGURE 6. Wave packet forcing: Fourier spectrum of (a) the perturbation streamfunction at the critical layer (b) the perturbation density at the critical layer at $t = 10$ (dashed lines) and $t = 100$ (solid lines). Parameters: $\varepsilon = 0.05$, $\lambda = 0.1$, $\mu = 0.2$, $Ri_c = 2$. At early time (the dashed lines), most of the contribution to the disturbance comes from wavenumbers in the neighbourhood of the forced wavenumber ($\kappa = \pm 2$). At late time (the solid lines), the contribution from the zero wavenumber becomes large, higher harmonics develop and the peaks at $\kappa = \pm 2$ become smaller.

in the vicinity of the forced wavenumber and the range of higher wavenumbers. In figure 8, these three components of the streamfunction are shown: in (a), the function $\psi_0(\mu x, z, t)$; in (b), the part of the disturbance centred at the forced wavenumber ($|\kappa| = 2$), calculated by inverting the transform over the interval $1 < |\kappa| < 3$ and, in (c), the part arising from the higher wavenumbers, i.e. $|\kappa| > 3$. All three quantities are evaluated at the critical level. In each graph, the corresponding quantity at early time ($t = 10$) is shown by the dashed line. It is clear from these graphs that the horizontal extent of the region in which the packet interacts with the basic flow increases in length with time. However, while the zero wavenumber component increases greatly in magnitude, the amplitude of the contribution from the forced wavenumber is actually smaller at late time than at early time.

Campbell (2003) examined the problem of a Rossby wave packet propagating on a horizontal plane. It was found there that the net absorption of the disturbance was prolonged owing to an increase in the longitudinal extent of the packet; however, there

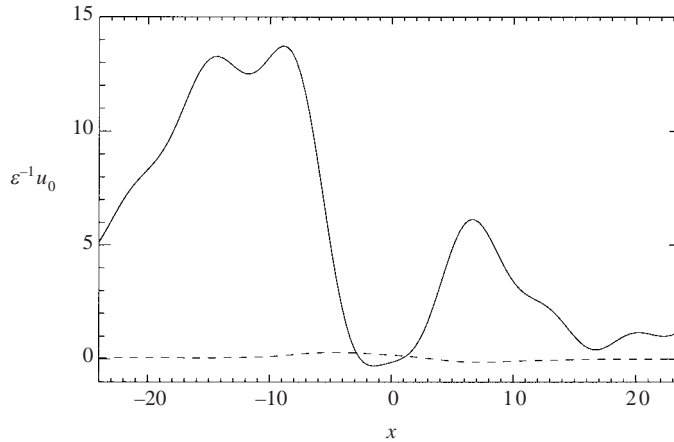


FIGURE 7. Wave packet forcing: variation of $u_0(x, z, t)$ with x at the critical level and at $t = 10$ (dashed line) and $t = 100$ (solid line). Parameters: $\varepsilon = 0.05$, $\lambda = 0.1$, $\mu = 0.2$, $Ri_c = 2$. $u_0(x, z, t)$ is the component of the disturbance arising from wavenumbers in the vicinity of the zero wavenumber. At early time $t = 10$, u_0 is approximately proportional to $\exp\{-2\mu^2 x^2\}$. By $t = 100$, it has increased by several orders of magnitude and is asymmetric in x .

was a different mechanism for this. The increased length of the packet in that problem was mainly due to a contribution from the wavenumbers in the neighbourhood of the forced wavenumber rather than the zero wavenumber. An explanation for this difference can be provided by examining the leading-order analytic solution to each of the two problems. In the gravity wave packet problem, the magnitude of the leading-order component of the term corresponding to the forced wavenumber $|\psi_1|$ varies like $|z - z_c|^{1/2}$ as $z \rightarrow z_c$, according to the early-time solution (B9). However, the wave-induced mean flow increases like t in the outer region, as noted in Appendix B.

Now the nonlinear critical layer for gravity waves has been shown to have a thickness of $\varepsilon^{2/3}$ (Maslowe 1972) and the time scale for the nonlinear terms to increase to the same order of magnitude as the linear terms is $t \sim O(\varepsilon^{-2/3})$ (Brown & Stewartson 1982). In this space-time regime ($|z - z_c| \sim O(\varepsilon^{2/3})$ and $t \sim O(\varepsilon^{-2/3})$), it follows that $\psi_0 \sim \varepsilon^2 t \sim O(\varepsilon^{4/3})$ and $\varepsilon \psi_1 \sim \varepsilon |z - z_c|^{1/2} \sim O(\varepsilon^{4/3})$, so the two components are of the same order of magnitude. With a monochromatic forcing, the mean flow term does not continue to increase with time after $t \sim O(\varepsilon^{-2/3})$; it oscillates between periods of growth and decay and thus, in the long time mean, it remains of the same order of magnitude as the periodic part of the disturbance. However, with the spatially localized forcing, since the momentum flux jump remains positive, the mean flow term continues to grow with time even after the onset of the nonlinear time regime and it would be expected to dominate for large t .

In contrast, in the Rossby wave packet problem, the critical-layer thickness is $\varepsilon^{1/2}$ and the nonlinear time regime starts when $t \sim O(\varepsilon^{-1/2})$ (Warn & Warn 1978). At the boundary of the critical layer, the component of the disturbance corresponding to the forced wavenumber is $O(1)$. The zero wavenumber term also increases like t . Thus, in the regime where $|y| \sim O(\varepsilon^{1/2})$ and $t \sim O(\varepsilon^{-1/2})$, $\varepsilon \psi_1$ is $O(\varepsilon)$ and $\psi_0 \sim \varepsilon^2 t \sim O(\varepsilon^{3/2})$. So, in contrast to the gravity wave packet problem, the contribution from the forced wavenumber continues to dominate the zero wavenumber term even in the nonlinear time regime and it will continue to do so at least until such time as $t \sim O(\varepsilon^{-1})$. This is seen in figure 5 of Campbell (2003).

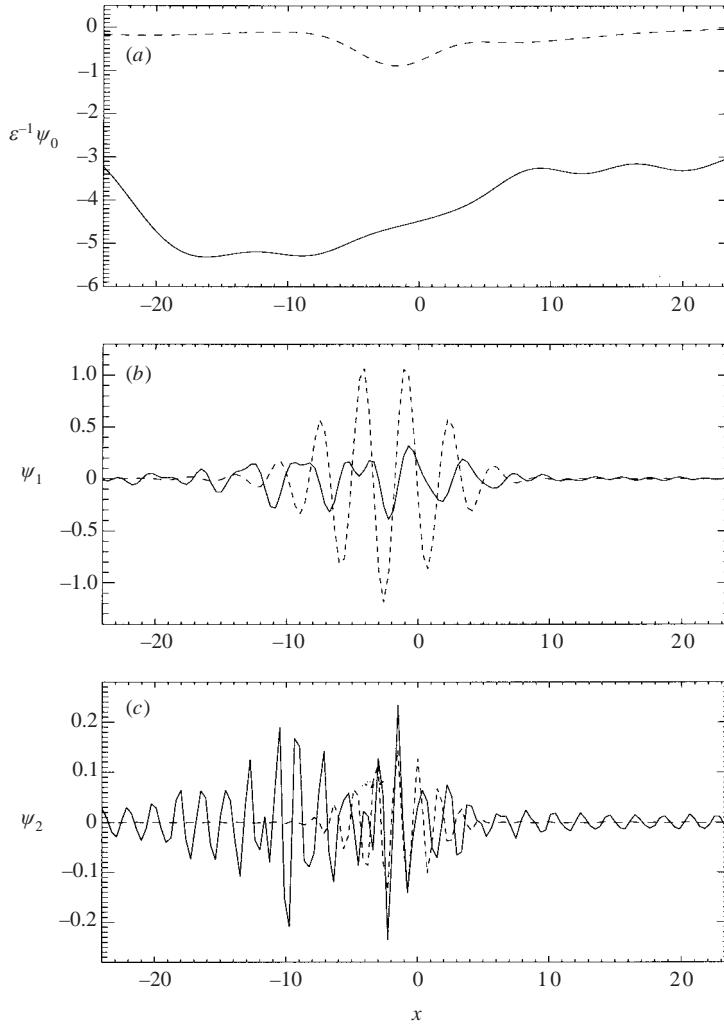


FIGURE 8. Wave packet forcing: perturbation streamfunction at the critical level ($z=0$) at $t=10$ (dashed lines) and $t=100$ (solid lines) decomposed into the part centred (a) at the zero wavenumber, (b) at the forced wavenumber and (c) the contribution from the higher harmonics. Parameters: $\varepsilon=0.05$, $\lambda=0.1$, $\mu=0.2$, $Ri_c=2$. All three components of the disturbance increase in horizontal extent at late time. The component ψ_1 due to the forced wavenumber, shown in (b), decreases in magnitude with time, while the other two components increase.

Another important point to note from figures 7 and 8 is that, at early time, \bar{u}_0 and $\bar{\psi}_0$ (the dashed lines) are approximately proportional to $\exp(-2\mu^2x^2)$, as noted in Appendix B. At late time, the outward propagation of the disturbance is primarily in the direction of positive x . One of the conclusions of the asymptotic analysis in Appendix B is the presence of terms proportional to $\exp(-\mu^2(x - \bar{u}(z)t)^2)$ and $\exp(-\mu^2(x - \bar{u}(z_1)t)^2)$. These describe wave packets propagating horizontally with phase speeds of $\bar{u}(z)$ and $\bar{u}(z_1)$, respectively. The disturbances with phase speeds $\bar{u}(z)$ would of course be stationary at the critical level, but those with phase speed $\bar{u}(z_1)$ propagate in the direction of negative x at all levels. Since these disturbances are superimposed upon disturbances with amplitudes of $\exp(-\mu^2x^2)$ and $\exp(-2\mu^2x^2)$, the result is that the overall disturbance is asymmetric in x at late time.

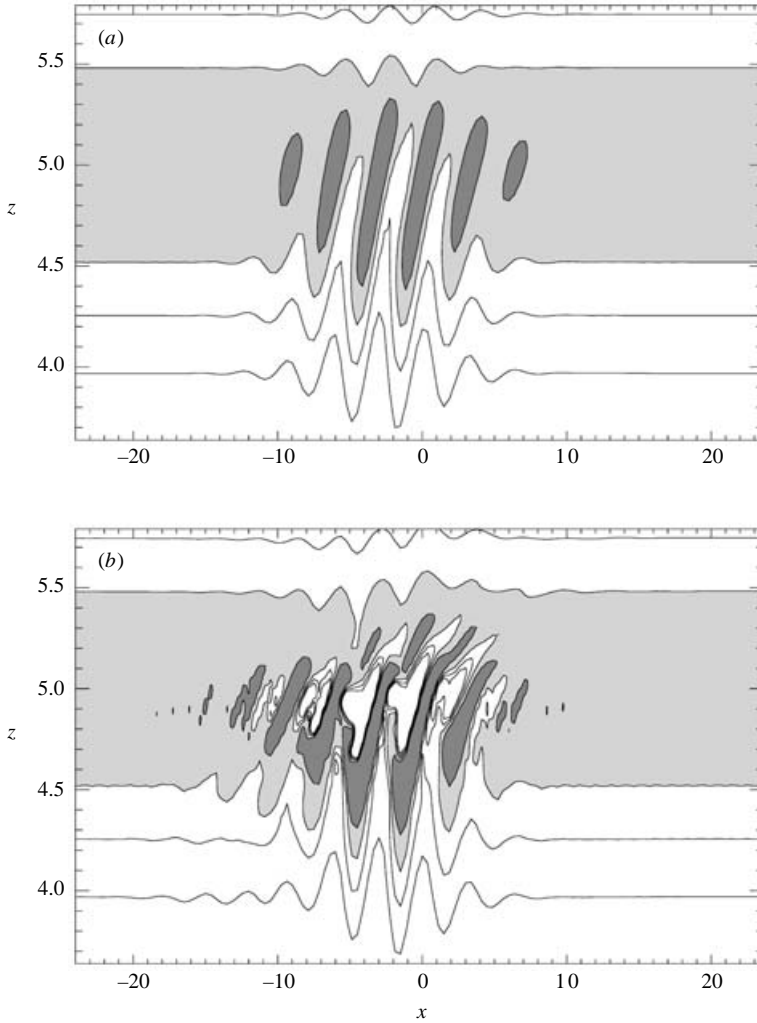


FIGURE 9. Wave packet forcing: total vorticity $\xi_{total} = \bar{\psi}_{zz} + \varepsilon \nabla^2 \psi$ in the critical layer at (a) $t = 10$ and (b) $t = 100$. Parameters: $\varepsilon = 0.05$, $\lambda = 0.1$, $\mu = 0.2$, $Ri_c = 2$. The dark grey shading indicates regions where $\xi_{total} < -1$, the light grey shading regions where $-1 < \xi_{total} < -0.8$ and $\xi_{total} > -0.8$ elsewhere. At early time (a), closed contours or cat's eyes are seen in the vicinity of the critical level. These features become deformed at late time (b) as the vorticity contours overturn.

The two contour plots in figure 9 show the total vorticity $\bar{\psi}_{zz} + \varepsilon \nabla^2 \psi$ at early and late times. At early time, the vorticity contours show the characteristic cat's eye structures observed in problems of this type. Since the forcing is localized in the horizontal direction, there is a train of cat's eyes whose size decreases away from the centre of the packet. The breakdown of the cat's eyes at late time is seen in figure 9(b). In the next two figures, density contours at early and late times have been shown for both types of forcing. Note that with the wave packet forcing, there are no actual density overturns even at late time (figure 10b), although there is evidence of these in the corresponding plot for the periodic case (figure 11b).

To investigate the instabilities resulting from the changes in density, we examine the evolution of the local Richardson number in the critical layer. This is based on

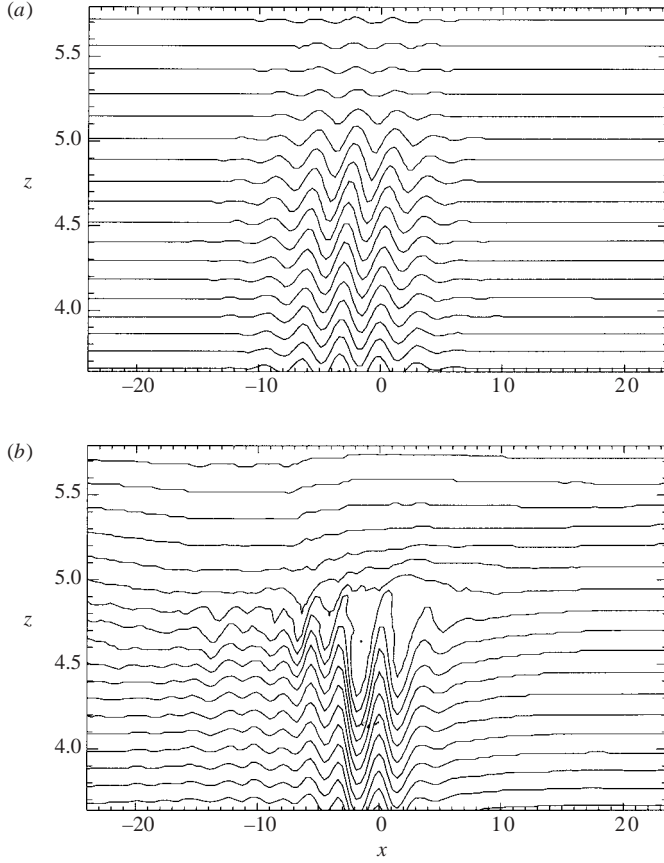


FIGURE 10. Wave packet forcing: total density $\rho_{total} = \bar{\rho} + \varepsilon\rho$ in the critical layer at (a) $t = 10$ and (b) $t = 100$. Parameters: $\varepsilon = 0.05$, $\lambda = 0.1$, $\mu = 0.2$, $Ri_c = 2$. Contour levels range from $\rho_{total} \approx 0.48$ at the bottom of each plot in equally spaced intervals to $\rho_{total} \approx 0.3$ at the top.

the velocity and density profiles taking the perturbation into account:

$$Ri = \frac{-g(\partial(\bar{\rho} + \varepsilon\rho)/\partial z)}{\bar{\rho}(\partial(\bar{u} + \varepsilon u)/\partial z)^2}. \quad (3.5)$$

Filled contours of the local Richardson number at levels $Ri = 0, 1/4$ have been added to the density contours in figure 11(b). The dark grey shading represents the regions where $Ri < 0$, the light grey shading the regions where $0 < Ri < 1/4$ and everywhere else $Ri > 1/4$. There are significant regions where the Richardson number is negative and the $Ri = 0$ contours are quite close to the $Ri = 1/4$ contours. In contrast, with the wave packet forcing, the Richardson number never goes below zero and there are only a few extremely small regions where it does go below $1/4$, so there is nothing to add to figure 10(b).

3.3. The effect of varying μ , ε and Ri_c

To examine the effect of varying the horizontal length of the forcing, the experiments described in the previous section were repeated with $\mu = 0.1, 0.4$ and 0.8 , while keeping the other parameters fixed at their standard values, $\varepsilon = 0.05$, $\lambda = 0.1$ and $Ri_c = 2$. In the absence of the nonlinear terms, the thickness of the critical layer would

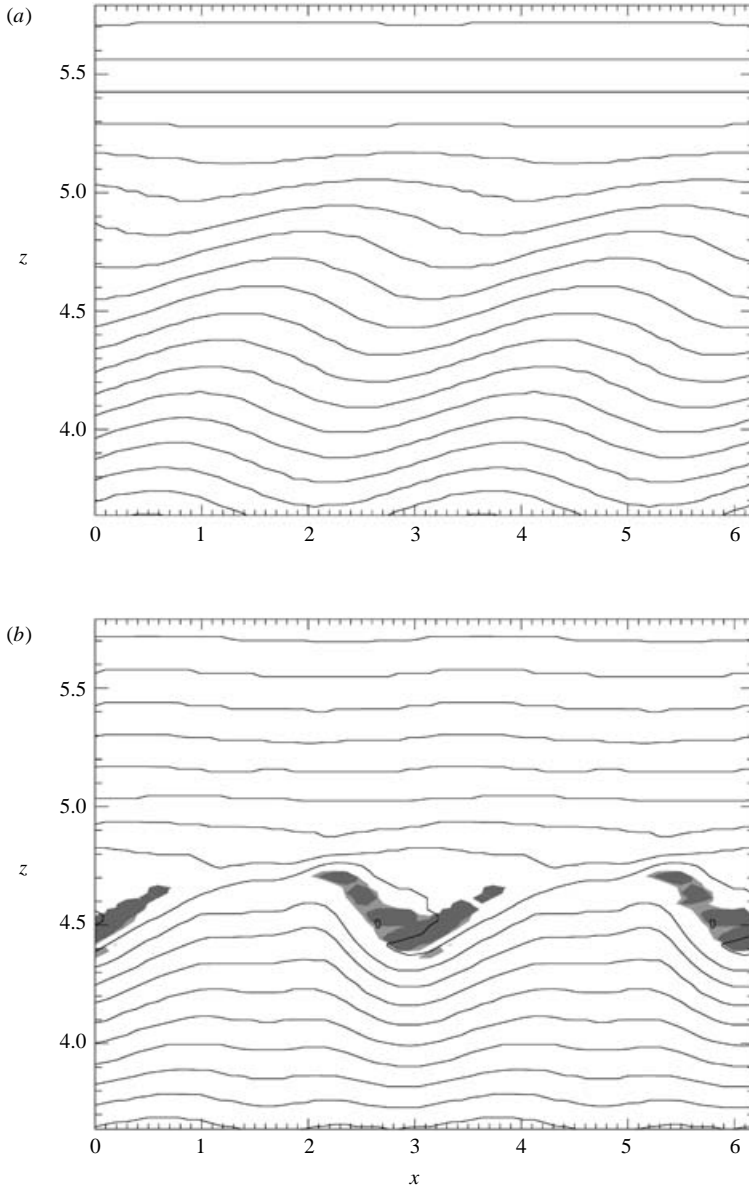


FIGURE 11. Monochromatic forcing: total density $\rho_{total} = \bar{\rho} + \varepsilon\rho$ in the critical layer at (a) $t = 10$ and (b) $t = 100$. Parameters: $\varepsilon = 0.05$, $\lambda = 0.1$, $Ri_c = 2$. Contour levels range from $\rho_{total} \approx 0.48$ at the bottom of each plot in equally spaced intervals to $\rho_{total} \approx 0.3$ at the top. In (b), the local Richardson number is shown by the shaded regions: $Ri < 0$ in the dark grey regions, $0 < Ri < 1/4$ in the light grey regions and $Ri > 1/4$ elsewhere. Note overturning of the density contours at late time (b).

be determined by the length scale of the packet. The linear wave packet critical-layer thickness would be μ (see Appendix B). When both wave packet and nonlinear terms are present, as in our simulations, their relative importance then depends on the magnitude of the ratio $\Lambda = \mu/\varepsilon^{2/3}$ of the wave packet critical-layer thickness to the nonlinear critical-layer thickness. With the values of μ used in this series of experiments, the ratio Λ would be changed from its value in the standard run

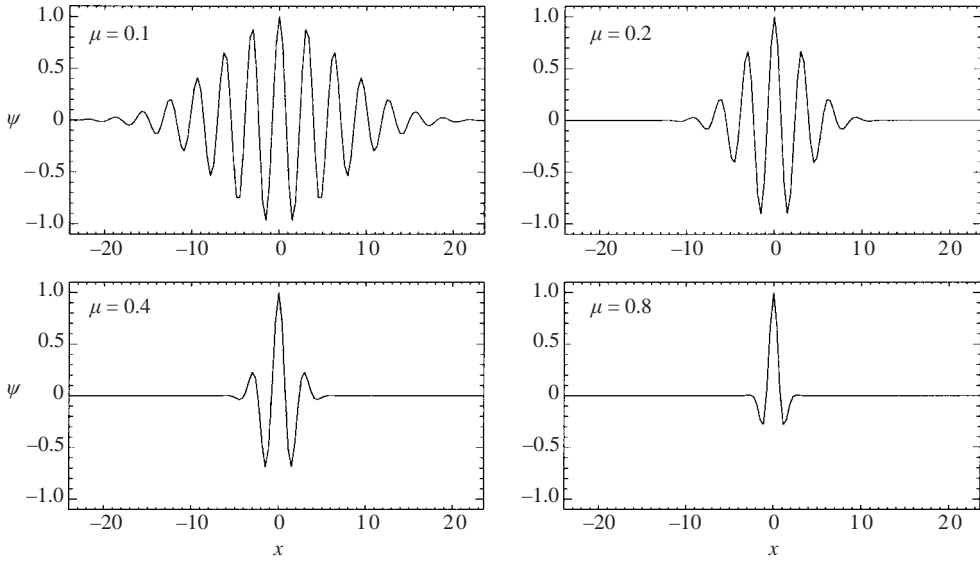


FIGURE 12. Wave packet forcing: perturbation streamfunction ψ at the forced boundary for different values of μ . The $\mu = 0.2$ curve is that used in the standard run. The time evolution of the jump in the momentum flux for each of these values of μ is shown in figure 13.

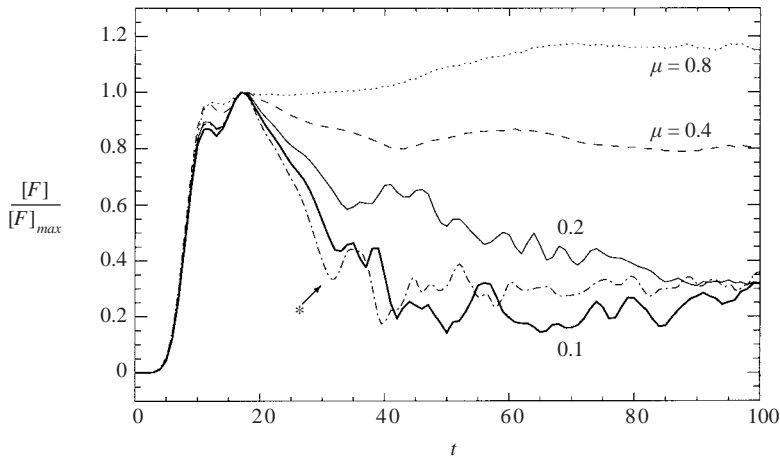


FIGURE 13. Effect of varying the horizontal length of the forcing: variation of the jump in the (normalized) momentum flux with t for different values of μ for fixed ε . Parameters: $\varepsilon = 0.02$, $\lambda = 0.1$, $\mu = 0.1, 0.2, 0.4, 0.8$, $Ri_c = 2$. The $\mu = 0.2$ curve shows the results of the standard run. Increasing μ gives a larger jump, i.e. increased net absorption. The curve labelled with an asterisk was obtained using a horizontally localized forcing with an x -independent amplitude.

by factors of 1/2, 2 and 4, respectively. The form of the forcing for each value of μ is shown in figure 12. For the simulations with $\mu = 0.1$, a longer computational domain ($-30 \leq x \leq 30$) was used. For each μ , the normalized momentum flux jump $[F]/[F]_{max}$ was calculated and plotted as a function of time. These graphs are shown in figure 13. It is evident that the magnitude of $[F]$ relative to $[F]_{max}$ (the maximum value it attains during the linear stage of evolution) depends directly on the value of μ . For small μ , $[F]/[F]_{max}$ decreases at late time and eventually attains a steady

state. However, in contrast to the monochromatic case, it never actually decreases to zero and absorption continues to dominate. With large μ , $[F]/[F]_{max}$, after an initial decrease at the end of the linear regime, starts to increase at late time and by the end of the simulation it has exceeded its linear value of 1. The reason that this is possible is that the horizontal extent of the packet in the critical layer has increased considerably at this time.

With our configuration, even when the length of the packet at the forced boundary is small (large μ), there is hardly any transmission of wave activity through the critical layer. This is in contrast to the case investigated by Javam & Redekopp (1998) in which the forcing is limited to a finite horizontal region, but with an amplitude independent of x in this region. They found that a packet of this form would be reflected or transmitted through the critical layer rather than being absorbed.

In their study, the disturbance is generated by means of a forcing term added to the governing equations for the velocity and the forcing is localized in height as well as in x , so their configuration is quite different from ours. Also their disturbance propagates downwards, rather than upwards, and the phase speed of their forcing is non-zero. In spite of these differences, we decided that it would be worth carrying out some simulations with a forcing function that is similar to theirs, i.e. with an x -independent amplitude. By doing that, we could rule out the possibility that the shape of the amplitude function affects the amount of transmission and that our results only hold when the amplitude function is Gaussian. Re-written in our notation, their forcing function is proportional to

$$\exp(ik(x - ct)) \exp(-\beta|z - z_2|^3) f(x) + \text{c.c.}, \quad (3.6)$$

where

$$f(x) = \begin{cases} 1, & |x| \leq M\pi/2k, \\ 0, & |x| > M\pi/2k. \end{cases} \quad (3.7)$$

The parameter M measures the horizontal extent of the forcing region in units of half-wavelengths and is assumed to be an odd number. The forcing is centred above the critical layer at a level which we have denoted as z_2 here, and β determines its vertical extent. The packet propagates downwards with a phase speed of $c = 1$. In our notation, the initial mean velocity profile used by Javam & Redekopp would be written as $\bar{u} = 1 - \tanh \alpha_0(z - z_c)$, where α_0 is a constant.

We carried out a series of experiments with this type of forcing, but using our configuration in which $\bar{u} = \tanh \alpha_0(z - z_c)$, $c = 0$, the forcing is applied at the lower boundary and the disturbance propagates upwards. The parameter β in (3.6) was set to zero. The parameter M was set to 9 to give a forcing region of just over 14 horizontal units, with k set to 2. All other parameters were chosen to be the same as those used in our standard run ($\varepsilon = 0.05$, $\lambda = 0.1$, $Ri_c = 2$). As in our previous simulations, the packet was absorbed at the critical level at early time and at late time there was some reflection, though very little transmission. There was a discontinuity in the vertical momentum flux across the critical layer and its evolution with time is shown in figure 13, compared with the 4 curves obtained with the Gaussian forcing. This last experiment was repeated with smaller values of M , making the packet more compact, as done in Javam & Redekopp's simulations, but absorption was still found to dominate transmission and reflection. We can conclude from these experiments that there is no qualitative difference between the results obtained with the two types of localized forcing; assuming a constant amplitude within the localized region, rather than a slowly varying Gaussian amplitude, does not have a significant effect on the

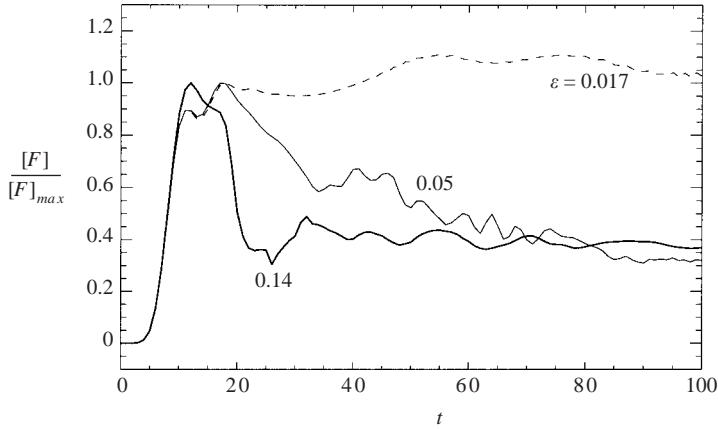


FIGURE 14. Effect of varying the amplitude of the forcing: variation of the jump in the (normalized) momentum flux with t for different values of the nonlinear parameter ε for fixed μ . Parameters: $\mu=0.2$, $\lambda=0.1$, $\varepsilon=0.017, 0.05, 0.14$, $Ri_c=2$. The $\varepsilon=0.05$ curve shows the results of the standard run. Reducing ε gives a larger jump, i.e. increased net absorption.

results. So the difference in the amount of transmission between our results and those of Javam & Redekopp is due not to the difference in the forcing amplitude function, but rather to the more fundamental differences in the configuration mentioned in the preceding paragraph, e.g. the vertical localization of their forcing.

In our next set of experiments, the amplitude of the forcing ε was varied while μ was kept fixed at a value of 0.2 and all the other parameters were also kept at their standard values. To change the ratio Λ by a factor of 1/2 while keeping μ constant, ε must be changed by a factor of $2^{3/2}$ or approximately 2.8. Results obtained using $\varepsilon=0.017, 0.05$ and 0.14 are shown in figure 14. With small ε , there is much greater net absorption and so there is no decrease in the jump in the momentum flux from its linear value. The jump attains a quasi-steady state with small-amplitude oscillations in time. For large ε , we would expect an earlier onset of the nonlinear regime (Brown & Stewartson 1982) and would also expect the nonlinear effects to dominate over the wave packet effects and, consequently, that the results would more closely resemble those in the monochromatic case. These predictions are confirmed by the $\varepsilon=0.14$ curve in figure 14. The decrease in the momentum flux jump occurs earlier than in the $\varepsilon=0.05$ run and the net absorption of the packet is greatly reduced, although the jump still remains positive.

Experiments with larger forcing amplitudes (up to $\varepsilon=0.5$) were also carried out. These were the only cases in which there was a non-negligible amount of wave activity transmitted beyond the critical layer. With large ε , the amplitude of the disturbance at the critical layer grows large, because the zero-wavenumber component grows with time (see Appendix B), and at large time it can even be of the same order of magnitude as the amplitude of the forcing. Consequently, the magnitude of the disturbance beyond the critical layer also becomes $O(1)$. Eventually, the linear radiation condition fails and the part of the disturbance that is transmitted beyond the critical layer reaches the upper boundary and is reflected. The interactions between the waves reflected at the upper boundary and the upward-propagating transmitted waves very soon lead to numerical instabilities. To prevent this problem, a radiation condition taking into account nonlinearities would be required.

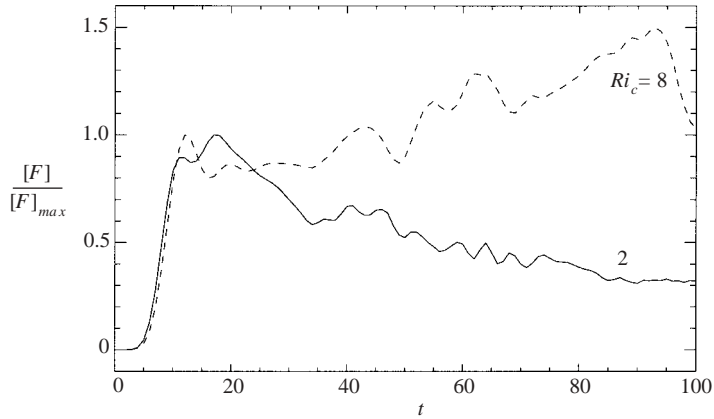


FIGURE 15. Effect of varying the initial Richardson number Ri_c : variation of the jump in the (normalized) momentum flux with t for different values of Ri_c for fixed μ and ε . Parameters: $\mu = 0.2$, $\lambda = 0.1$, $\varepsilon = 0.05$, $Ri_c = 2, 8$. The $Ri_c = 2$ curve shows the results of the standard run. To obtain the $Ri_c = 8$ curve, the background shear is reduced by a factor of 2. Increasing Ri_c gives a larger jump, i.e. increased net absorption, as predicted by Booker & Bretherton's linear solution.

Finally, we investigated the effect of varying the local Richardson number. The shear of the mean flow was decreased by a factor of 2 to give $Ri_c = 8$. According to the linear solution of Booker & Bretherton (1967), the magnitude of the discontinuity in the vertical momentum flux increases with increasing Ri_c . This was seen to be the case in our nonlinear simulations as well; larger values of Ri_c result in greater net absorption at late time, as shown in figure 15.

4. Conclusions

In this paper, the effect of a wave packet forcing on a nonlinear gravity wave critical layer has been investigated. It was seen that the spatial localization reduces reflection to the extent that absorption dominates and the jump in the total vertical momentum flux does not go to zero even at large time. This is because the zero-wavenumber component of the disturbance and the contributions from the wavenumbers in the immediate vicinity of the zero wavenumber increase in magnitude and horizontal extent with time. This outward flux of wave activity in the horizontal direction and the prolonged absorption of the disturbance are similar to what was observed in Bacmeister & Pierrehumbert's (1988) study of waves forced by flow over an isolated mountain. It must be noted, however, that the problem they studied differs from ours in several ways. In the mountain wave configuration, the coordinates follow the shape of the mountain, a drag force is exerted on the mountain by the flow and there is a jump in the flow characteristics across the length of the mountain (analogous to the 'hydraulic jump' in the theory of hydrostatic flow described, for example, by Baines 1995). Waves are generated on the lee-side of the mountain and propagate downstream. In our study, the prescribed lower boundary condition forces a disturbance which propagates vertically upward and the concept of a hydraulic jump does not apply. Considering these differences, the similarity between our results and theirs is noteworthy.

Our numerical simulations show that the extent of absorption relative to reflection depends on the amplitude and horizontal length of the forcing, as well as on the

strength of the mean shear in the vicinity of the critical layer. Results obtained with a constant-amplitude localized forcing were qualitatively the same as those obtained using a forcing function with a slowly varying Gaussian amplitude. For a given shape of amplitude function, decreasing the horizontal length of the packet at the source level had the effect of increasing the net absorption of the packet at the critical layer. Increasing the amplitude of the forcing had the effect of reducing the extent of absorption relative to reflection, while increasing the Richardson number by decreasing the mean shear caused greater net absorption. None of our simulations resulted in a significant degree of transmission of the disturbance through the critical layer; the horizontally averaged vertical momentum flux was in all cases approximately zero above the critical layer.

It was also noted that the local Richardson number did not at any time become negative anywhere in the flow domain and, although there were some regions in which $0 < Ri < 1/4$, these were negligibly small. In contrast, in the case of monochromatic forcing, substantial regions with $0 < Ri < 1/4$ and $Ri < 0$ appeared at large time and there was evidence of overturns in the density contours.

The evolution of the gravity wave packet critical layer may be compared with that in the case examined by Campbell (2003) of a Rossby wave packet propagating southwards in a horizontal plane. In that problem, the longitudinal extent of the disturbance was seen to increase with time both in the critical layer and in the outer region. The numerical experiments carried out here revealed that the distortion of the mean flow is much larger relative to the magnitude of the perturbation in the gravity wave problem than in the Rossby wave problem. A consequence of this is that the nature of the interaction between the packet and the mean flow differs in the two problems. In the gravity wave packet case, we have seen that the part of the disturbance that spreads out is centred at the zero wavenumber; in the case of the Rossby wave packet, on the other hand, there is a greater contribution from higher wavenumbers in the neighbourhood of the wavenumber of the forcing. A comparison of the different components of the disturbance in each problem was carried out by examining the leading-order terms in the respective analytic solutions. These approximate solutions give us a general idea of how the disturbance evolves with time.

There are a number of questions arising from the results of the numerical simulations which could be answered by a complete asymptotic analysis of the late-time nonlinear gravity wave packet critical layer, along the lines of that carried out by Brown & Stewartson (1982), but including the effects of the wave packet forcing. An outline of the procedure is given in Appendix B. Important points to address include the x -dependence of the disturbance in the inner and outer regions and the mechanism by which the disturbance increases in horizontal extent with time.

A number of other possibilities would arise from extending the model used in our simulations to take into account variations in all three dimensions. For the case of orographically-forced waves, Shutts (1995, 1998) points out that, while the assumption of two-dimensionality may be justified for flow over a long mountain ridge, it is important to include a third dimension for flow over an isolated mountain, since the disturbance would then be comprised of contributions from all angles.

In a nonlinear problem such as that studied here, even if the disturbance is two-dimensional initially, there is the possibility of the development of three-dimensional instabilities. Using the results of their two-dimensional nonlinear numerical simulations, Lin *et al.* (1993) noted that the most unstable mode would be a spanwise instability (out of the plane of the shear), thus confirming the importance of including

three-dimensional dynamics in representing the critical-layer breakdown. Winters & D'Asaro (1994) carried out nonlinear three-dimensional numerical simulations for the case of a vertically localized and initially two-dimensional gravity wave packet and contrasted their results with those obtained in a two-dimensional configuration. They found that the early-time evolution of the critical layer was similar to that in the two-dimensional case, but at late time, transverse convective instabilities developed. In these investigations, however, the disturbance was monochromatic in the horizontal direction. It would be of interest to examine the three-dimensional evolution of a horizontally localized packet such as that employed in the present paper.

The authors are grateful to Dr G. Brunet and Dr T. Warn for helpful discussions on nonlinear critical layers and to the three anonymous referees whose comments led to several improvements in the paper. L.J.C. wishes to acknowledge the Zonta International Foundation for support in the form of an Amelia Earhart Fellowship during the time this research was being carried out.

Appendix A. The radiation condition

At the upper boundary of the computational domain, the disturbance is assumed to be small enough that the nonlinear terms may be neglected and a radiation condition derived. Near this boundary, the basic flow velocity may be treated as a constant, $\bar{u} \approx 1$ and $\bar{u}_{zz} \approx 0$. For steady linear monochromatic waves, the radiation condition is then simply

$$\phi_z \pm im\phi = 0, \quad (\text{A } 1)$$

from the Taylor–Goldstein equation, (3.3), with $m^2 \approx N^2/\bar{u}^2 - \delta k^2$. For a time-dependent wave packet, a radiation condition may be obtained by linearizing equations (2.1) and (2.3) and taking a Fourier transform in x and then a Laplace transform in t , as was done by B eland & Warn (1975) for the case of time-dependent Rossby waves. The result is

$$\tilde{\psi}_{zz} - \left[\frac{N^2 \kappa^2}{(s + i\kappa\bar{u})^2} + \delta \kappa^2 \right] \tilde{\psi} = 0, \quad (\text{A } 2)$$

where $\tilde{\psi}(\kappa, z, s)$ is the Fourier–Laplace transform of $\psi(x, z, t)$. In order to be able to obtain bounded solutions to this equation as $z \rightarrow \infty$, we require that

$$\tilde{\psi}_z + H(\kappa, s)\tilde{\psi} = 0, \quad (\text{A } 3)$$

where $H(\kappa, s)$ is the square root of the expression in square brackets. On re-writing this in the form,

$$H(\kappa, s) = \delta^{1/2} \kappa \left[\frac{(s + i\kappa\bar{u})^2 + N^2/\delta}{(s + i\kappa\bar{u})^2} \right]^{1/2}, \quad (\text{A } 4)$$

it is seen that the inverse Laplace transform of H is given by

$$h(\kappa, t) = \frac{N^2 \kappa}{\delta^{1/2}} \int_0^t \frac{a}{\tau} \mathcal{J}_1(a\tau) d\tau e^{-i\kappa\bar{u}t} + \delta^{1/2} \kappa e^{-i\kappa\bar{u}t} \delta(t - 0), \quad (\text{A } 5)$$

where \mathcal{J}_1 is the Bessel function of order 1, $\delta(t - 0)$ is the delta function and the constant $a = N^2 \kappa / \delta$. Inverting the Laplace transform gives an equation for $\hat{\psi}(\kappa, z, t)$,

the Fourier transform of $\psi(x, z, t)$, in terms of a convolution integral,

$$\hat{\psi}_z + \int_0^t \hat{\psi}(\kappa, z, \tau)h(t - \tau) d\tau. \quad (\text{A } 6)$$

This can be written as

$$\hat{\psi}_z + \delta^{1/2}\kappa\hat{\psi} = -\delta^{1/2}\kappa \int_0^t \hat{\psi}(\kappa, z, \tau)g(t - \tau) e^{-i\kappa\bar{u}(t-\tau)} d\tau, \quad (\text{A } 7)$$

where

$$g(t) = \int_0^t \frac{a}{\eta} \mathcal{J}_1(a\eta) d\eta. \quad (\text{A } 8)$$

The radiation condition can be simplified if we make use of the fact that $\delta \ll 1$; then H can be approximated by

$$H(\kappa, s) = \frac{N\kappa}{s + i\kappa\bar{u}}, \quad (\text{A } 9)$$

so that

$$h(\kappa, t) = N\kappa e^{-i\kappa\bar{u}t}. \quad (\text{A } 10)$$

Appendix B. Asymptotic analysis

Some aspects of the asymptotic analysis that are relevant to interpreting and understanding the results of the numerical simulations are presented here. To examine the evolution of the critical layer and the outer region, we first simplify equations (2.1)–(2.3) by neglecting the viscous and heat conduction terms. Let us assume also that the basic flow has constant shear; in the vicinity of the critical layer, this is a valid approximation for the hyperbolic tangent mean profile used in the numerical simulations. The configuration corresponding to that used in the standard run is $\bar{u} = z - z_c$. In the absence of the nonlinear, viscous and heat conduction terms, equations (2.1)–(2.3) can be combined to give the single equation,

$$\left(\frac{\partial}{\partial t} + \bar{u} \frac{\partial}{\partial x} \right)^2 \nabla^2 \psi + N^2 \psi_{xx} = 0. \quad (\text{B } 1)$$

We first note that for a steady disturbance in normal mode form, the amplitude of the perturbation streamfunction is given by (3.3), which has linearly independent solutions,

$$\phi_A \sim (z - z_c)^{1/2+i\gamma} \quad (\text{B } 2)$$

and

$$\phi_B \sim (z - z_c)^{1/2-i\gamma}, \quad (\text{B } 3)$$

with $\gamma = (Ri_c - 1/4)^{1/2}$. The general solution is the linear combination,

$$\phi = a\phi_A + b\phi_B, \quad (\text{B } 4)$$

where a and b are constants. These solutions are valid in the outer region and are discontinuous across the critical layer and, as a result, there is a phase change of $-\pi$ (Miles 1961).

As a starting point for the analysis, we re-examine the linear inviscid solution to the time-dependent problem obtained by Booker & Bretherton (1967) with a monochromatic forcing and then add the effects of nonlinearity and spatial-localization. By taking a Laplace transform in time of equation (B 1), they found expressions for

the perturbation in the outer region (equations 5.2, 5.6 and 6.1 in their paper) and in the inner region (equation 5.9). To leading order, the perturbation in the outer region takes the form

$$\psi \sim e^{ikx} \left\{ h(z) + e^{-ik\tilde{z}t} \left(\frac{h_A(z)}{t^{3/2+i\gamma}} + \frac{h_B(z)}{t^{3/2-i\gamma}} \right) \right\} + \text{c.c.}, \quad (\text{B } 5)$$

where

$$h(z) = a\tilde{z}^{1/2} \mathcal{J}_{i\gamma}(k\tilde{z}) + b\tilde{z}^{1/2} \mathcal{J}_{-i\gamma}(k\tilde{z}). \quad (\text{B } 6)$$

The functions $\mathcal{J}_{\pm i\gamma}(k\tilde{z})$ are modified Bessel functions of complex order, $h_A(z)$ and $h_B(z)$ are also expressions involving modified Bessel functions, $\gamma = (Ri_c - 1/4)^{1/2}$, and we have denoted $(z - z_c)$ by \tilde{z} . There are additional terms in the solution which were not given explicitly by Booker & Bretherton; they result from the various singularities that arise in the process of evaluating the inverse Laplace transform (p. 529 of their article). With the forcing applied at the level $z = z_1$, there are two additional time-dependent terms that are of interest to us; they are proportional to $\exp(-ik(z_1 - z_c)t) t^{3/2 \pm i\gamma}$. To leading order in \tilde{z} , the first term in (B 6) is equal to ϕ_A and the second term to ϕ_B . As $t \rightarrow \infty$, the steady solution (B 4) results. Booker & Bretherton showed that the ϕ_A term corresponds to an upward-travelling wave and the ϕ_B term to a downward-travelling wave. With the forcing applied below the critical level, the first term is dominant, it is reduced by a factor of $e^{-2\pi\gamma}$ across the critical layer and the horizontally averaged momentum flux is given by

$$F(z, t) = \begin{cases} -\frac{\gamma}{2k} |a|^2 e^{2\gamma\pi}, & z < z_c, \\ \frac{\gamma}{2k} |a|^2, & z > z_c. \end{cases} \quad (\text{B } 7)$$

Booker & Bretherton's analysis can be generalized to the case in which the forcing is of the form $\exp(ikx) \exp(-\mu^2 x^2)$. The solution procedure follows that employed by Campbell & Maslowe (1998) for the linear inviscid Rossby wave packet problem; it involves taking a Fourier transform in x as well as a Laplace transform in time of the linear equation (B 1) to give

$$(s + i\kappa\tilde{z})^2 (\tilde{\psi}_{zz} - \delta\kappa^2 \tilde{\psi}) + N^2 \kappa^2 \tilde{\psi} = 0, \quad (\text{B } 8)$$

where $\tilde{\psi}(\kappa, z, s)$ is the Fourier-Laplace transform of $\psi(x, z, t)$. With this forcing function, most of the contribution to the solution comes from a small neighbourhood of wavenumbers κ around the central wavenumber $\kappa = k$ and we can take advantage of that to obtain a solution in powers of $(\kappa - k)$. After inverting the transforms, a solution in powers of μ is obtained. To leading order, the solution is of the form $\psi \sim \psi^{(0)}(x, z, t) + O(\mu^2)$. It would be complicated to obtain the exact expression for the $O(\mu^2)$ term; however, for the present discussion, it suffices to know the form of the leading-order term $\psi^{(0)}(x, z, t)$. This would necessarily take the form of Booker & Bretherton's monochromatic solution multiplied by the factor $\exp(-\mu^2 x^2)$, i.e.

$$\psi^{(0)} \sim \exp(-\mu^2 x^2) \exp(ik_x) \left\{ h(z) + \exp(-ik\tilde{z}t) \left(\frac{h_A(z)}{t^{3/2+i\gamma}} + \frac{h_B(z)}{t^{3/2-i\gamma}} \right) \right\} + \text{c.c.} \quad (\text{B } 9)$$

Thus, to leading order, the qualitative behaviour of the solution is not significantly different from that obtained with the monochromatic forcing. This was seen in the numerical simulations; when $\varepsilon = 0$, the spatial-localization of the forcing does not affect the qualitative behaviour of the solution. Since it is at this order that the discontinuity in the solution appears, it follows that the phase change is still $-\pi$, as in the monochromatic case. The appropriate scaled variables in this linear problem

are the slow variables μx and μt and the critical-layer variable $\mu^{-1}\tilde{z}$. The linear wave packet critical-layer thickness is μ^{-1} .

If ε is non-zero in the governing equations, then the effects of nonlinearity must be taken into account. Assuming that $\varepsilon \ll 1$, then the solution can be expressed in powers of ε , at least at early time, and the expression for $\psi^{(0)}$ given in (B 9) represents the leading-order term in the series. We can write

$$\psi \sim \psi^{(0)} + \varepsilon\psi^{(1)} + O(\mu^2). \tag{B 10}$$

When this is substituted into the nonlinear inviscid equations, along with a similar expression for the perturbation density, it is found that $\psi^{(1)}$ must contain a term proportional to $\exp(-2\mu^2x^2)$, corresponding to the low wavenumbers, and a term proportional to $\exp(2ikx)\exp(-2\mu^2x^2)$, corresponding to the higher wavenumbers. These two terms correspond to the quantities shown in figures 8(a) and 8(c) respectively.

At early time, the momentum flux $\hat{F}(\kappa, z, t)$ for each wavenumber κ takes the form (B 7), with k replaced by κ and with a a function of κ instead of a constant. The total momentum flux $F(z, t)$ is the integral of $\hat{F}(\kappa, z, t)$ over the range of wavenumbers κ . Now the evolution of the mean flow, in the absence of viscosity, is governed by

$$\frac{\partial \bar{u}_0}{\partial t} = \varepsilon^2 \frac{\partial F}{\partial z}, \tag{B 11}$$

which gives, on integrating with respect to z and t ,

$$\bar{\psi}_0(z, t) = -\varepsilon^2 \int_0^t F(z, \tau) d\tau, \tag{B 12}$$

i.e. the wave-induced mean streamfunction is proportional to the time-integrated vertical momentum flux. At early time, F is independent of t and so the mean streamfunction increases like t in the outer region.

The solution (B 10) is valid in the regime where $t < O(\varepsilon^{-2/3})$. To examine the long-time (fully nonlinear) evolution of the disturbance in the outer region using multiple scaling, we would have to define a slow time scale $T = \varepsilon^{2/3}t$, as well as a slow spatial scale $X = \mu x$, and obtain a late-time solution in terms of these variables. The question then arises as to the relative magnitude of the two small parameters ε and μ . The simplest balance would be that in which the widths of the two critical layers (the linear wave packet critical layer and the nonlinear critical layer) are assumed to be the same, i.e. the balance $\varepsilon^{2/3} = \mu$. The governing equations written in terms of the slow variables $T = \varepsilon^{2/3}t$ and $X = \varepsilon^{2/3}x$ yield a series of linear equations that can be solved to obtain the form of the late-time solution. This solution is then matched for $T \rightarrow 0$ with the early-time solution.

The solution procedure is analogous to that of Brown & Stewartson (1982), the main difference being that, with the localized forcing, each equation would contain additional terms involving derivatives with respect to the slow scale X , i.e. each derivative with respect to T would be replaced by the operator $(\partial/\partial T + \bar{u}(\partial/\partial X))$. A consequence of this is that terms in the monochromatic solution that are proportional to $\exp(-ik(z - z_c)t)$ and $\exp(-ik(z_1 - z_c)t)$ would be proportional to

$$\exp(-(X - (z - z_c)T)^2) \exp(ik(x - (z - z_c)t)) \tag{B 13}$$

and

$$\exp(-(X - (z_1 - z_c)T)^2) \exp(ik(x - (z_1 - z_c)t)) \tag{B 14}$$

instead. These expressions describe wave packets propagating outwards with phase speeds determined by the basic flow velocity in the interior of the flow, $\bar{u}(z) = z - z_c$, and at the forced boundary, $\bar{u}(z_1) = z_1 - z_c$. The part of the disturbance given by (B 13) propagates in the direction of positive/negative x above/below the critical level and has zero phase speed at the critical level. However, the phase speed of the part given by (B 14) does not depend on height and is thus negative even at the critical level. Finally, we note that these terms give rise to low-wavenumber terms that are proportional to $\exp(-(X - (z - z_c)T)^2)$ and $\exp(-(X - (z_1 - z_c)T)^2)$. The results of the numerical simulations (figures 2, 7, 8 and 9) show that, in the critical layer and below, the disturbance propagates outwards and in the direction of negative x .

REFERENCES

- BACMEISTER, J. T. & PIERREHUMBERT, R. T. 1988 On high-drag states of nonlinear stratified flow over an obstacle. *J. Atmos. Sci.* **45**, 63–80.
- BAILEY, D. H. & SWARZTRAUBER, P. N. 1991 The fractional Fourier transform and applications. *SIAM Rev.* **33**, 389–404.
- BAILEY, D. H. & SWARZTRAUBER, P. N. 1994 A fast method for the numerical evaluation of continuous Fourier and Laplace transforms. *J. Sci. Comput.* **15**, 1105–1110.
- BAINES, P. 1995 *Topographic Effects in Stratified Flows*. Cambridge University Press.
- BÉLAND, M. & WARN, T. 1975 The radiation condition for transient Rossby waves. *J. Atmos. Sci.* **32**, 1873–1880.
- BOOKER, J. R. & BRETHERTON, F. P. 1967 The critical layer for gravity waves in a shear flow. *J. Fluid Mech.* **27**, 513–539.
- BROWN, S. N. & STEWARTSON, K. 1982, On the nonlinear reflexion of a gravity wave at a critical level, Part 3. *J. Fluid Mech.* **115**, 231–250.
- BRUNET, G. & HAYNES, P. H. 1996 Low-latitude reflection of Rossby wave trains. *J. Atmos. Sci.* **53**, 482–496.
- CAMPBELL, L. J. 2000 Nonlinear critical layer development of forced wave packets in geophysical shear flows. PhD thesis, McGill University.
- CAMPBELL, L. J. 2003 Wave-mean-flow interactions in a forced Rossby wave packet critical layer. *Stud. Appl. Maths* (to appear).
- CAMPBELL, L. J. & MASLOWE, S. A. 1998 Forced Rossby wave packets in barotropic shear flows with critical layers. *Dyn. Atmos. Oceans* **28**, 9–37.
- CAMPBELL, L. J. & MASLOWE, S. A. 2001 A numerical simulation of the nonlinear critical layer evolution of a forced Rossby wave packet in a zonal shear flow. *Math. Comput. Simulation* **55**, 365–375.
- CLARK, T. & PELTIER, W. R. 1984 Critical level reflection and the resonant growth of nonlinear mountain waves. *J. Atmos. Sci.* **41**, 3122–3134.
- ELIASSEN, A. & PALM, E. 1961 On the transfer of energy in stationary mountain waves. *Geophys. Publ.* **22**, 1–23.
- FRITTS, D. C. 1982 The transient critical level interaction in a Boussinesq fluid. *J. Geophys. Res.* **87**, 7997–8016.
- HOWARD, L. N. 1961 Note on a paper of John W. Miles. *J. Fluid Mech.* **10**, 509–512.
- JAVAM, A. & REDEKOPP, L. G. 1998 The transmission of spatially-compact internal wave packets through a critical level. *Dyn. Atmos. Oceans* **28**, 127–138.
- LELE, S. K. 1992 Compact finite difference schemes with spectral-like resolution. *J. Comput. Phys.* **103**, 16–42.
- LIN, C.-L., FERZIGER, J. H., KOSEFF, J. R. & MONISMITH, S. G. 1993 Simulation and stability of two-dimensional internal gravity waves in a stratified shear flow. *Dyn. Atmos. Oceans* **19**, 325–366.
- MASLOWE, S. A. 1972 The generation of clear air turbulence by nonlinear waves. *Stud. Appl. Maths* **51**, 1–16.
- MILES, J. W. 1961 On the stability of heterogeneous flows. *J. Fluid Mech.* **10**, 496–508.

- PELTIER, W. R. & CLARK, T. 1979 The evolution and stability of finite amplitude mountain waves. Part II: surface wave drag and severe downslope windstorms. *J. Atmos. Sci.* **36**, 1498–1529.
- SHUTTS, G. 1995 Gravity-wave drag parametrization over complex terrain: The effect of critical-level absorption in directional wind-shear. *Q. J. R. Met. Soc.* **121**, 1005–1021.
- SHUTTS, G. 1998 Stationary gravity-wave structure in flows with directional wind shear *Q. J. R. Met. Soc.* **124**, 1421–1442.
- WARN, T. & WARN, H. 1978 The evolution of a nonlinear critical level. *Stud. Appl. Maths* **59**, 37–71.
- WINTERS, K. B. & D'ASARO, E. A. 1989 Two-dimensional instability of finite amplitude internal gravity wave packets near a critical level. *J. Geophys. Res.* **94**, 12 709–12 719.
- WINTERS, K. B. & D'ASARO, E. A. 1994 Three-dimensional instability near a critical level. *J. Fluid Mech.* **272**, 255–284.